Electronic Supporting Information for the manuscript

Unusual Slow Magnetic Relaxation in a Sulfate-Bridged Copper (II) Complex with 1-(2-Pyridylazo)-2-Naphthol Ligand

Meriem Goudjil[a,b*], Carlo Andrea Mattei[c], Leonardo Tacconi[c], Laura Chelazzi[d], Mauro Perfetti[e*]

[a] Department of Industrial Engineering, University of Florence, Via Santa Marta 3, Florence 50139, Italy
[b] Institute of Nanostructured Materials (ISMN) – National Research Council (CNR), Via P. Gobetti 101, Bologna, 40129 Italy
[c] Department of Chemistry "U. Schiff", University of Florence, Via della Lastruccia 3-13, Sesto Fiorentino, 50019, Firenze, Italy
[d] Centro di Cristallografia Strutturale, University of Florence, Via della Lastruccia 3, Sesto Fiorentino, Florence 50019, Italy
[e] Department of Chemistry "U. Schiff", University of Florence and INSTM Research Unit, Via della Lastruccia 3-13, Sesto Fiorentino, 50019, Firenze, Italy

*Corresponding authors: meriem.goudjil@unifi.it, mauro.perfetti@unifi.it

Table of Content

1. Introduction

Table S1. CCDC survey of PAN transition-metal complexes: monomers.

Type	Refcode	Unit cell parameters	Composition	Reference
Monomers	AGOSAR	*P*-1, *a* = 8.774(9)Å, *b* = 12.685(12)Å, *c* = 12.883(13)Å *α* = 62.69(10)°, *β* = 75.07(9)°, *γ* = 82.15(8)°	bis(PAN)-Ru(ii)	1
	AGOSEV	*C*2/*c*, *a* = 30.611(4)Å, *b* = 11.6611(14)Å, *c* = 16.491(2)Å *α* = 90°, *β* = 114.595(13)°, *γ* = 90°	(PAN)-(2,2':6',2"-terpyridine)-Ru(II)·ClO_4	
	AGOSIV	*Cm*, *a* = 18.325(3)Å, *b* = 15.250(12)Å, *c* = 9.6397(8)Å *α* = 90°, *β* = 122.099(5)°, *γ* = 90°	(PAN)-bis(PPh_3)-chloro-Ru(II)·DCM solvate	
	AGOSOV	$P2_12_12_1$, *a* = 10.2654(9)Å, *b* = 13.2256(12)Å, *c* = 15.7074(14)Å	(PAN)-(2,2'-bipyridine)-chloro-Ru(II)	
	YOLNAP	*P*-1, *a* = 9.6460(19)Å, *b* = 13.208(3)Å, *c* = 14.071(3)Å *α* = 93.11(3)°, *β* = 94.88(3)°, *γ* = 102.59(3)°	bromo-bis(PAN)-Re(III)·TCM solvate	2
	YOLNET	*Pcab*, *a* = 14.1208(5)Å, *b* = 9.0866(3)Å, *c* = 39.4688(17)Å	chloro-bis(PAN)-Re(III)	
	LEKNIA	$P2_1/c$, *a* = 18.2245(15)Å, *b* = 7.2396(6)Å, *c* = 14.8995(13)Å *α* = 90°, *β* = 112.193(4)°, *γ* = 90°	Tricarbonyl-chloro-(PAN)-Re(I)	3
	LEKNUM	$P2_1/n$, *a* = 11.429(2)Å, *b* = 28.788(6)Å, *c* = 12.820(3)Å *α* = 90°, *β* = 112.00(3)°, *γ* = 90°	Carbonyl-(ethane-1,2-diylbis(DPP))-(PAN)-Re(I)·DCM solvate	
	FOLZOX	$P2_1/c$, *a* = 8.583(4)Å, *b* = 16.929(7)Å, *c* = 19.659(8)Å *α* = 90°, *β* = 99.892(5)°, *γ* = 90°	Chloro-(η^5-pentamethyl-cyclopentadienyl)-(PAN)-Rh(III)·TfO	4
	FOMBAM	*P*-1, *a* = 9.1279(17)Å, *b* = 11.394(2)Å, *c* = 16.825(3)Å *α* = 102.330(3)°, *β* = *96*.882(2)°, *γ* = *104*.537(2)°	(η^5-Pentamethyl-cyclopentadienyl)-aqua-(PAN)-Rh(III)·bis(TfO)	
	FOLZUD	*P*-1, *a* = 9.205(2)Å, *b* = 11.366(3)Å, *c* = 16.818(4)Å *α* = 95.568(2)°, *β* = *96*.745(3)°, *γ* = *96*.973(2)°	(η^5-Pentamethyl-cyclopentadienyl)-aqua-(PAN)-Ir(III)·bis(TfO)	
	TUSSEG	*P*-1, *a* = 10.8892(13)Å, *b* = 12.4195(14)Å, *c* = 14.1371(16)Å *α* = 90.479(2)°, *β* = 104.604(2)°, *γ* = 112.926(2)°	dichloro-(PAN)-(PPh_3)-Rh(III)·DCM solvate	5
	TUSSIK	*P*-1, *a* = 11.118(2)Å, *b* = 13.600(3)Å, *c* = 17.797(4)Å *α* = 91.01(3)°, *β* = 104.56(3)°, *γ* = 94.01(3)°	chloro-(PAN)-bis(PPh_3)-Rh(III)·PF_6·DCM solvate	
	CUPYZN	*P*-1, *a* = 10.38Å, *b* = 8.22Å, *c* = 9.35Å *α* = 85.33°, *β* = *96.80*°, *γ* = 93.32°	(PAN)-aqua-Cu(II)·ClO_4	6
	DAFKUQ	$P2_1/n$, *a* = 9.058(2)Å, *b* = 11.896(3)Å, *c* = 14.013(2)Å *α* = 90°, *β* = 108.65(2)°, *γ* = 90°	(PAN)-(nitrato-O)-Cu(II)	7
	DAFKUQ01	$P2_1/n$, *a* = 9.046(3)Å, *b* = 11.876(4)Å, *c* = 14.006(5)Å *α* = 90°, *β* = 108.792(4)°, *γ* = 90°	(PAN)-(nitrato-O)-Cu(II)	8
	KAKZIF	*P*-1, *a* = 11.945(1)Å, *b* = 13.630(3)Å, *c* = 7.651(2)Å *α* = 103.63(3)°, *β* = 92.09(3)°, *γ* = 84.43(2)°	(Phenanthroline-N,N')-(PAN)-Cu(II)·TFB	9
	KAKZOL	*P*-1, *a* = 9.342(7)Å, *b* = 10.356(5)Å, *c* = 8.208(5)Å *α* = 93.31(5)°, *β* = 95.01(6)°, *γ* = 83.33(5)°	aqua-(perchlorato-O)-(PAN)-Cu(II)	
	KAKZUR	*P*-1, *a* = 11.095(5)Å, *b* = 20.367(5)Å, *c* = 7.539(2)Å *α* = 96.13(2)°, *β* = 102.14(2)°, *γ* = 80.98(3)°	aqua-((TFB)-PAN)-Cu(II)·diaqua-(PAN)-Cu(II)·TFB	
	DILBEG	*P*-1, *a* = 11.5045(11)Å, *b* = 12.3189(11)Å, *c* = 12.5197(12)Å *α* = 95.568(2)°, *β* = *91*.851(2)°, *γ* = *96*.973(2)°	$[(HPAN)]^+[(PAN)\text{-tris(isothiocyanato)-Cr(III)}]^-$·MeOH solvate	10

Table S2. CCDC survey of PAN transition-metal complexes: dimers and coordination polymers.

Type	Refcode	Unit cell parameters	Composition	Reference
Dimers	PAZNCO	*Pcab*, a = 17.83Å, b = 21.48Å, c = 7.14Å	di-(μ_2-chloro)-bis(PAN-Cu(II))	11
	PAZNCO01	$P2_1/a$, a = 15.817(3)Å, b = 8.255(1)Å, c = 10.404(3)Å α = 90°, β = 103.46(2)°, γ = 90°		
	VAYMAJ	P-1, a = 8.488(7)Å, b = 10.100(7)Å, c = 11.974(12)Å α = 72.23(7)°, β = 78.56(7)°, γ = 73.55(6)°	bis((PAN)-(μ_2-oxo)-oxo-V(V)) hydrogen peroxide·TCM solvate	12
	VAYMEN	$P2_1/c$, a = 11.496(4)Å, b = 9.883(3)Å, c = 16.360(5)Å α = 90°, β = 100.18(5)°, γ = 90°	Pyridine-(PAN)-oxo-peroxo-V(V)	
	LEKNOG	P-1, a = 9.328(5)Å, b = 9.625(5)Å, c = 11.929(5)Å α = 83.557(5)°, β = 68.824(5)°, γ = 78.410(5)°	bis(μ_2-PAN)-hexacarbonyl-di-Re(I)·cyclohexane solvate	3
	ONETEH	P-1, a = 11.595(2)Å, b = 13.729(3)Å, c = 13.920(3)Å α = 64.864(2)°, β = 68.492(2)°, γ = 68.090(2)°	bis(μ_2-PAN)-tetrakis(theonyltrifluoroacetonato)-di-Eu(III)·1-chlorobutane·1,2-DCE solvate	13
	ONETIL	P-1, a = 12.1389(19)Å, b = 15.049(2)Å, c = 22.718(4)Å α = 101.147(2)°, β = 95.205(2)°, γ = 95.384(2)°	bis(μ_2-PAN)-tetrakis(theonyltrifluoroacetonato)-di-Gd(III)·ClBz solvate	
	ONETOR	P-1, a = 12.618(6)Å, b = 13.656(6)Å, c = 13.862(6)Å α = 114.775(5)°, β = 93.962(6)°, γ = 114.963(5)°	bis(μ_2-PAN)-tetrakis(theonyltrifluoroacetonato)-di-Yb(III)·ClBz solvate	
	ONETUX	P-1, a = 12.099(3)Å, b = 14.978(3)Å, c = 22.666(5)Å α = 101.088(2)°, β = 95.284(2)°, γ = 95.280(3)°	bis(μ_2-PAN)-tetrakis(theonyltrifluoroacetonato)-di-Tb(III)·ClBz solvate	
Coordination polymer	HAVHIY	$R3c$, a = 29.847(3)Å, b = 29.847(3)Å, c = 8.3903(9)Å α = 90.00, β = 90.00°, γ = 120.00°	catena-[(μ-iodo)-{PAN}-di-Cu(II)]	14

2. Spectral characterization

2.1. Infrared spectra

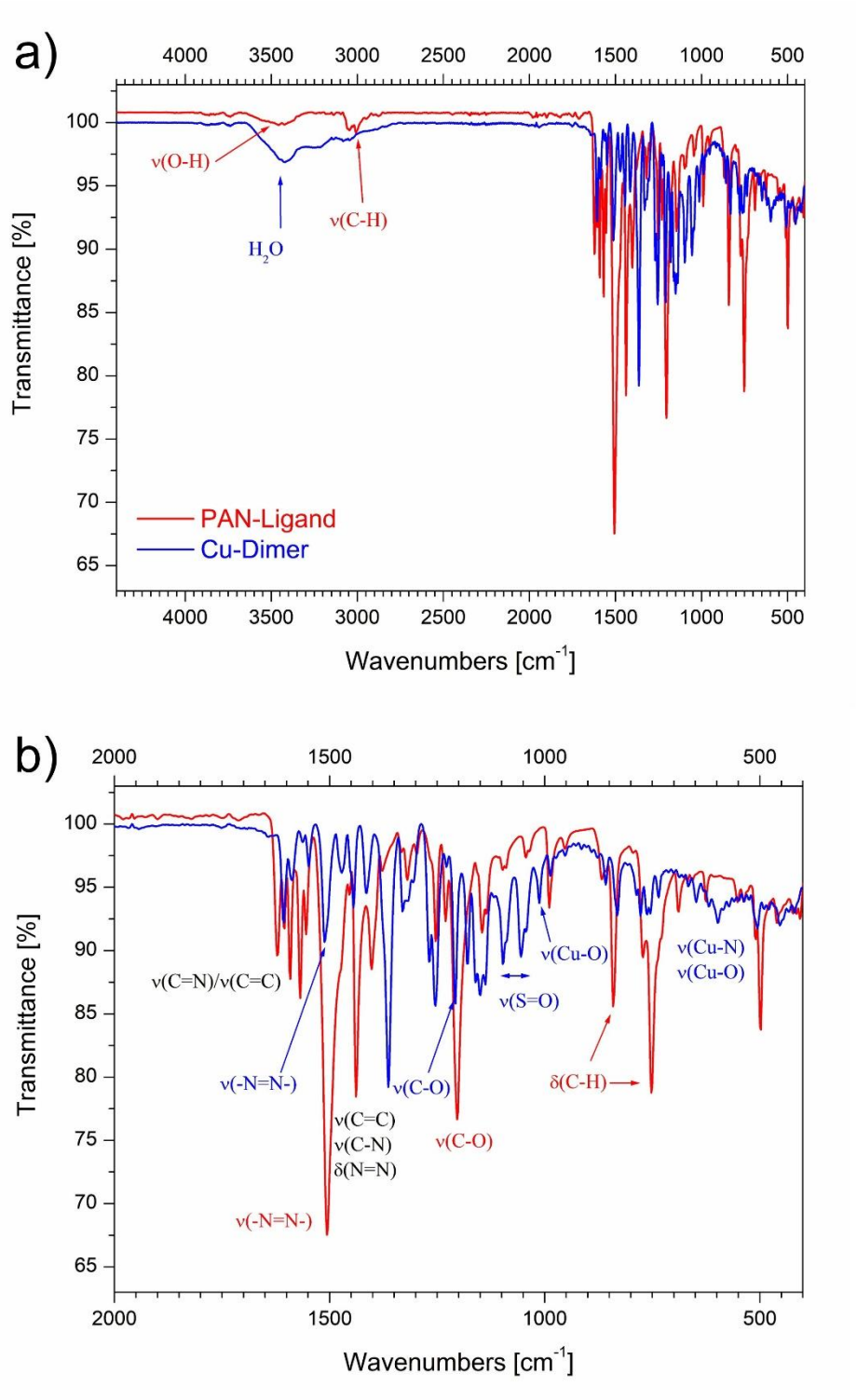

Figure S1. Infrared spectra of the PAN free ligand and its copper (II) dimer (a); enlarged view showing the characteristic vibrational modes (b).

2.2. UV-Vis spectra

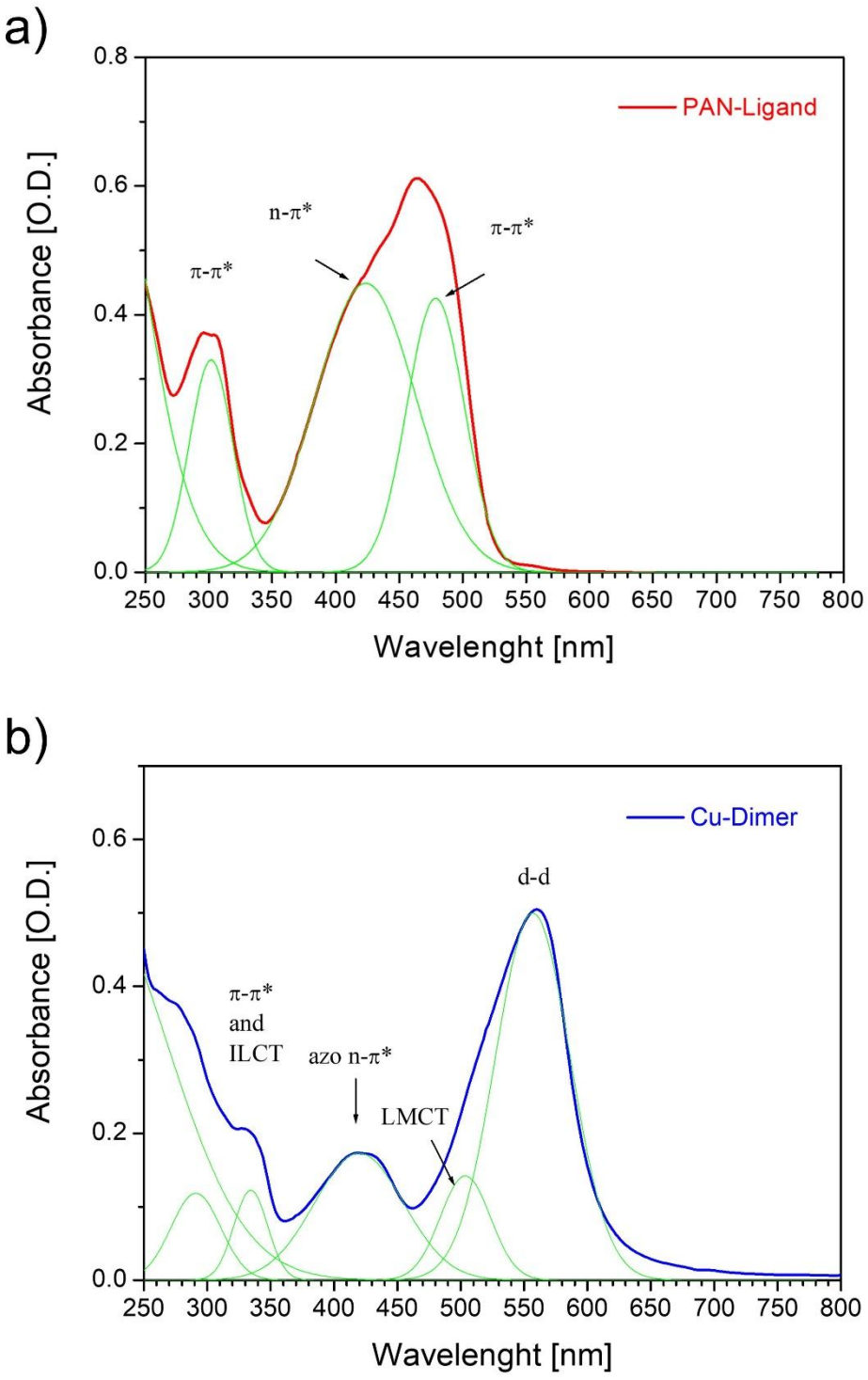

Figure S2. UV-Vis spectra in EtOH (10^{-6} M) of the free PAN ligand **(a)** and the Cu(II) dimer **(b)**.

3. X-ray diffraction studies

3.1. Single-crystal X-ray diffraction (SC-XRD)

From a total of 47897 measured reflections, 5229 unique were merged in the 2/*m* Laue group (R_{int} = 0.076). The intensity statistics test ($|E^2-1|$ = 0.963) suggested a centrosymmetric structure. Lattice symmetry and systematic absences analysis supported the $P2_1/n$ space group, in which the structure solution was undertaken. The crystal structure was solved using intrinsic-phasing method via the SHELXT program,[15] and refined by full-matrix least-squares methods on F^2 using SHELXL,[16] both implemented within the Olex 2 software suite.[17] All non-hydrogen atoms were refined anisotropically. Hydrogen atoms were positioned geometrically and refined using a riding model. Final refinement, based 5229 unique intensities and 429 parameters, converged at $R(F^2)$ = 0.050 (wR_2 = 0.145) for 4607 observed reflections with $F_o > 4\sigma(F_o)$. Crystallographic data and refinement details are summarized in Table S3. The complete dataset is available in the crystallographic information file (.CIF) from the Cambridge Crystallographic Data Centre (CCDC) under deposition number 2264081. Structural illustrations were prepared using CCDC Mercury (v. 2025.1.0).[18]

Table S3. Crystal data and structure refinement for μ-Sulfato-di-copper(II)-bis(1-(2-Pyridylazo)-2-naphtholate).

Crystal data	
Empirical formula	$C_{30}H_{24}Cu_2N_6O_8S$
Formula weight	755.69
Temperature/K	150(2)
Crystal system	monoclinic
Space group	$P2_1/n$
a (Å)	6.0802(3)
b (Å)	29.7530(13)
c (Å)	15.7206(6)
β/°	90.991(2)
V (Å)^3	2843.5(2)
Z	4
ρ_{calc} (g/cm^3)	1.765
μ (mm^{-1})	3.108
F(000)	1536.0
Crystal size/mm^3	0.140 × 0.020 × 0.020
Data collection	
Radiation	Cu $K\alpha$ (λ = 1.54178)
2θ range (°)	5.94–136.79
Index ranges	$-7 \le h \le 7$, $-35 \le k \le 35$, $-18 \le l \le 18$
Reflections collected	47897
Independent reflections	5229 [R_{int} = 0.0755, R_{sigma} = 0.0306]
Reflections obs. with $I \ge 2\sigma$ (I)	4607
T_{min}–T_{max}	0.670–0.753
sin(λ/θ)	0.603
Refinement	
Data/restraints/parameters	5229/0/429
Final R indexes [$I \ge 2\sigma$ (I)]	R_1 = 0.0503, wR_2 = 0.1438
Final R indexes [all data]	R_1 = 0.0568, wR_2 = 0.1482
Goodness-of-fit on F^2	1.086
Largest diff. peak/hole (e Å^{-3})	1.26/–1.45

Table S4. Selected bond lengths (Å) and angles (°) for $[Cu_2(\mu\text{-}SO_4)(PAN)_2(H_2O)_2]$.

Bond length (Å)					
Cu1—N1A	2.010(3)	Cu2—N1B	2.002(4)	S1—O1S	1.467(3)
Cu1—N3A	1.948(3)	Cu2—N3B	1.988(4)	S1—O2S	1.495(3)
Cu1—O1A	1.981(3)	Cu2—O1B	1.987(3)	S1—O3S	1.465(3)
Cu1—O1S	2.249(3)	Cu2—O2S	1.946(3)	S1—O4S	1.482(2)
Cu1—O1W	1.926(3)	Cu2—O2W	2.302(3)		
Bond angle (°)					
N1A—Cu1—N3A	79.19(13)	N1B—Cu2—N3B	78.48(15)	O1—S1—O2	108.43(17)
N3A—Cu1—O1A	82.42(12)	N3B—Cu2—O1B	80.95(12)	O1—S1—O3	111.46(17)
O1A—Cu1—O1W	96.88(12)	O1B—Cu2—O2W	94.46(13)	O1—S1—O4	109.26(16)
O1W—Cu1—N1A	98.45(13)	O2W—Cu2—N1B	94.36(12)	O2—S1—O3	109.89(17)
N1A—Cu1—O1S	94.95(12)	N1B—Cu2—O2S	101.11(15)	O2—S1—O4	108.52(18)
N3A—Cu1—O1S	92.62(11)	N3B—Cu2—O2S	167.97(13)	O3—S1—O4	109.23(17)
O1A—Cu1—O1S	96.47(11)	O1B—Cu2—O2S	97.46(13)		
O1W—Cu1—O1S	101.05(11)	O2W—Cu2—O2S	93.61(11)		
N1A—Cu1—O1A	158.73(12)	N1B—Cu2—O1B	158.14(14)		
N3A—Cu1—O1W	166.30(13)	N3B—Cu2—O2W	98.42(12)		

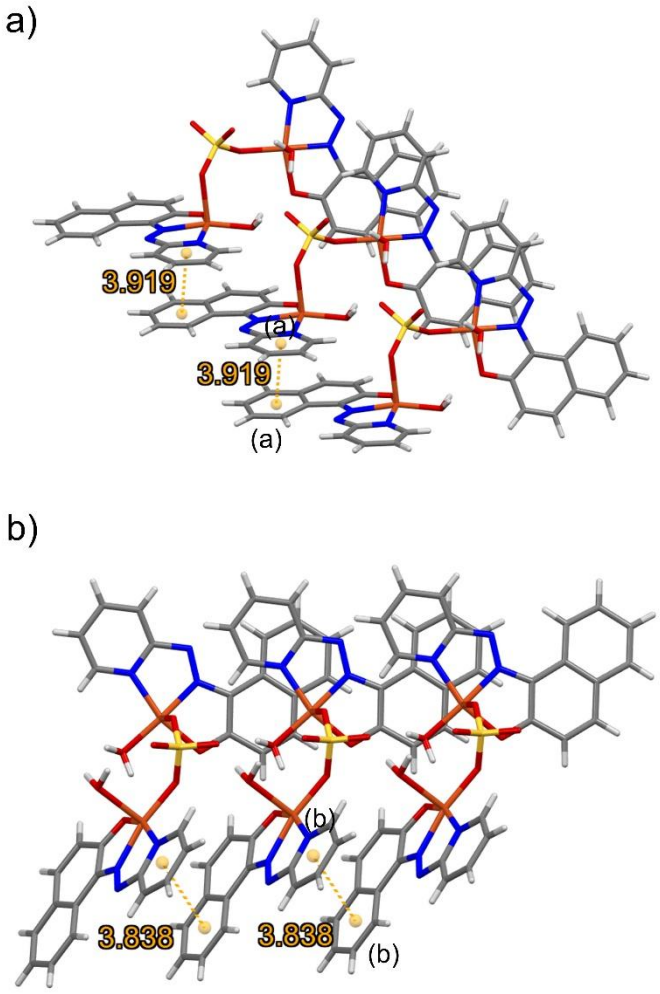

Figure S3. Views showing π–π stacking between the pyridyl and phenyl rings in $[Cu_2(\mu\text{-}SO_4)(PAN)_2(H_2O)_2]$.

3.2. Powder X-ray diffraction (P-XRD) data

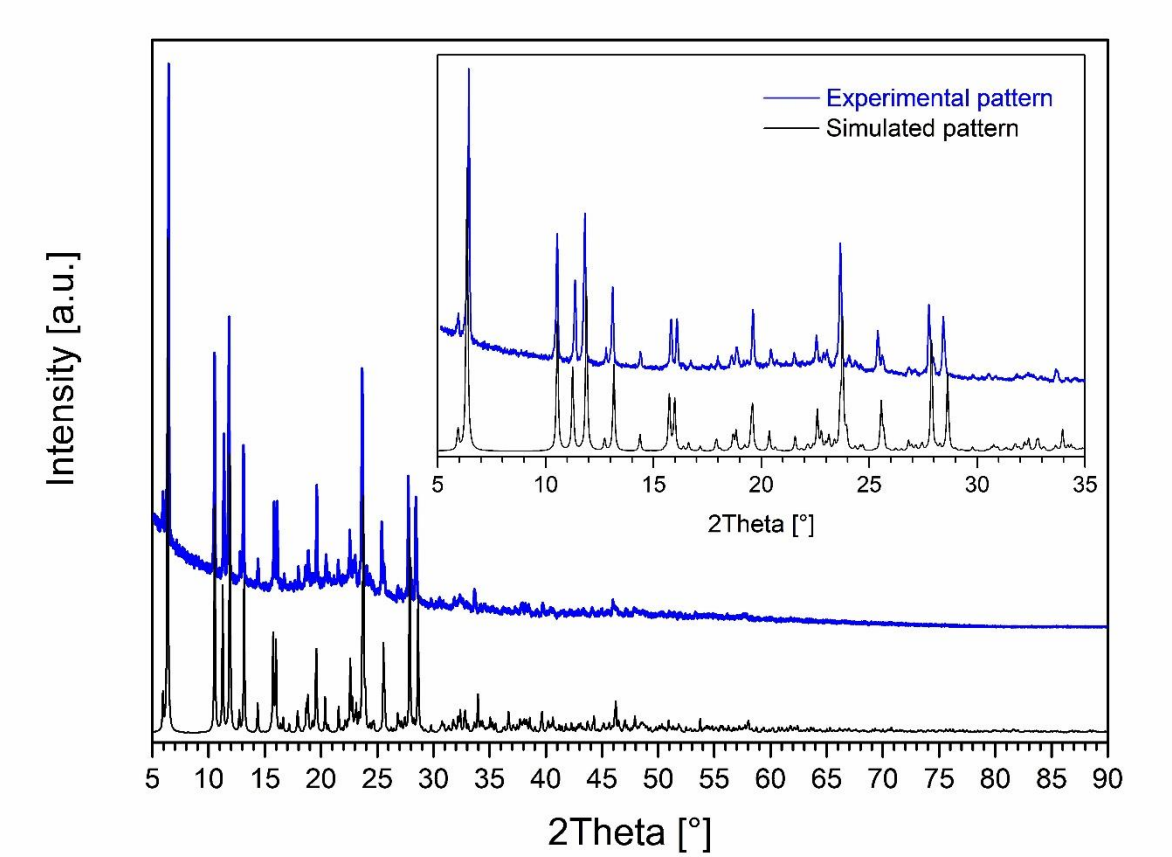

Figure S4. Overlay between the experimental (blue) and the calculated (black) P-XRD patterns for $[Cu_2(\mu\text{-}SO_4)(PAN)_2(H_2O)_2]$, revealing the high crystallinity and absence of impurities in the bulk sample. Inset: magnified view of the 2θ region from 5-35°, providing better comparison.

4. Hirshfeld surface analysis

To elucidate the strength and contribution of intermolecular interactions to the total packing, we performed HS analysis. The crystal packing of the copper (II) complex was further examined using CrystalExplorer (version 21.5, 608bb32),[19] which facilitated the generation of Hirshfeld surfaces (HSs) and their corresponding 2D fingerprint plots (FPPs). These analyses were computed using the structure's CIF as input. HSs were generated using a very high resolution. In the HSs mapped over d_{norm}, a red-blue-white color scheme is followed to visualize intermolecular interactions. White regions indicate contacts at distances equal to the sum of van der Waals (vdW) radii. At the same time, red spots highlight closer-than-expected contacts (indicative of significant interactions), and blue areas represent contacts longer than the vdW sum, suggesting weaker or non-bonding interactions.

The HS mapped over the d_{norm} (-0.619 to 1.489 a.u.), the shape index (-0.990 to 0.995 a.u.) and curvedness (-3.743 to 0.440 a.u.) is shown in Figure S5. The surfaces are rendered transparent to facilitate visualization of the underlying molecular structure.

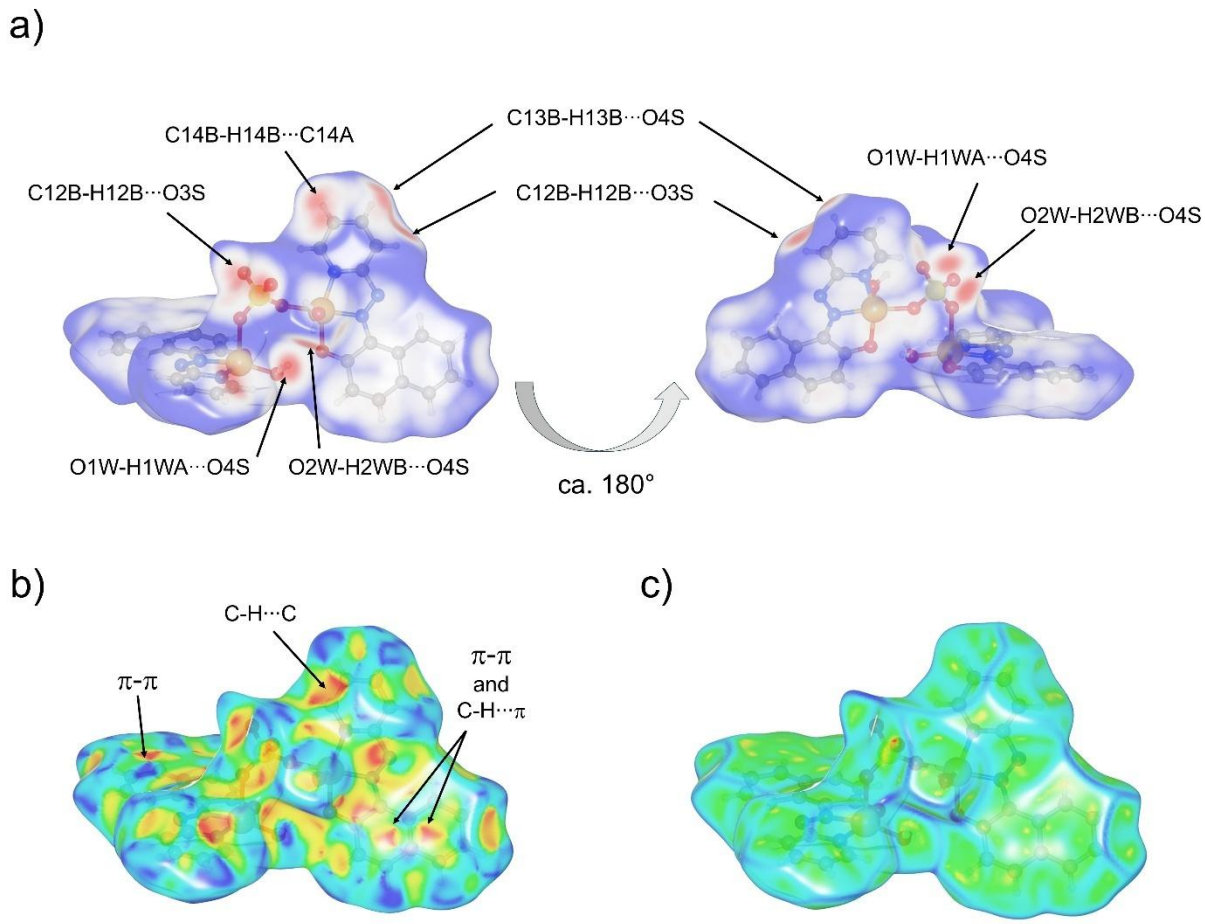

Figure S5. View of the 3D Hirshfeld surface in $[Cu_2(\mu\text{-}SO_4)(PAN)_2(H_2O)_2]$ plotted over d_{norm} (a), shape index (b) and curvedness (c).

Prominent red spots on the d_{norm} surface (Figure S5a) are attributed to O–H···O hydrogen bonds involving coordinated water molecules and the sulfone group (Figure S6a), as discussed in Section 3.2 (see manuscript, Figure 2a, Table 1). Additional red regions highlight short contacts between pyridine-ring hydrogens and sulfone oxygen atoms: C12B–H12B···O3S (1.905 Å, 120.9°) and C12B–H12B···O4S (2.117 Å, 167.7°), shown in Figure S6b. Another red spot corresponds to a C–H···C interaction between inequivalent pyridine rings (C14B–H14B···C14A at 2.425 Å; Fig.S6c). The presence of C–H···π and π–π interactions is supported by complementary blue and orange triangular patterns on the shape index surface (Fig.S5b), which correspond to the relatively flat green regions on the curvedness surface (Fig.S5c).

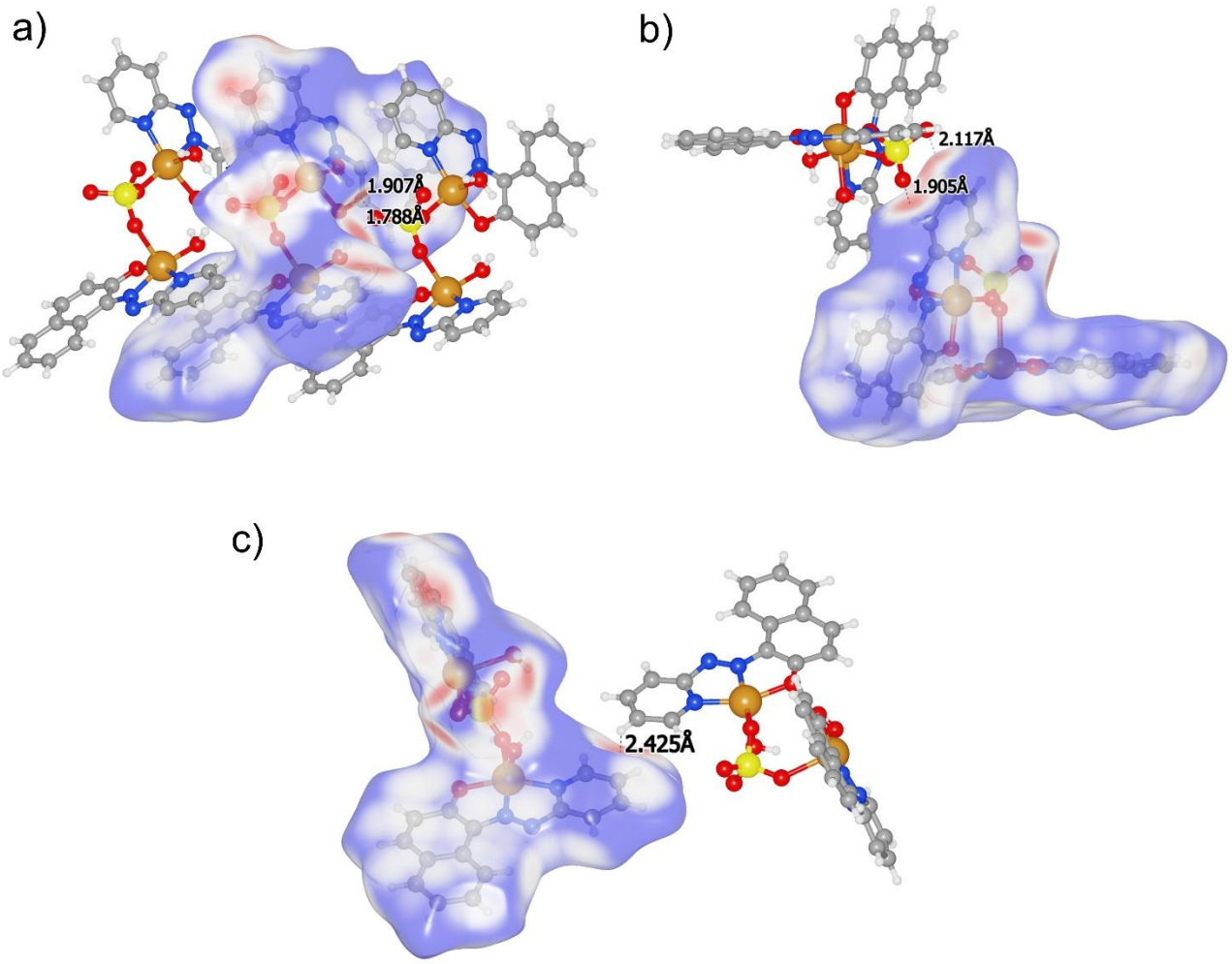

Figure S6. Intermolecular interactions visualized using Hirshfeld surfaces mapped over d_{norm} in μ-Sulfato-di-copper(II)-bis(1-(2-Pyridylazo)-2-naphtholate): O···H bonding contacts involving sulfone-water **(a)**; CH-sulfone **(b)**, and CH···C **(c)** interactions involving pyridyl rings.

Structural intermolecular interactions, such as π–π stacking, C–H···O, and O–H···O hydrogen bonds, as well as paramagnetic metal cations, have been proposed as potential pathways for magnetic super-exchange via noncovalent interactions.[20] Among these, particular emphasis has been placed on π–π interactions.[21] Quantitative analysis via 2D fingerprint plots reveals that H···H contacts are the most prevalent, contributing 35.5% to the total HS, followed by C···H/H···C (23.8%) and O···H/H···O (21.0%). The latter form a pair of sharp spikes with *di*+*de* = 1.75 Å, see Fig.S7, due to the robust water-sulfone H-bond interactions. Minor contributions arise from C···N/N···C (6.0%), N···H/H···N (4.5%), and C···C (π–π stacking) interactions (3.7%), highlighting the multifaceted nature of the crystal packing forces.

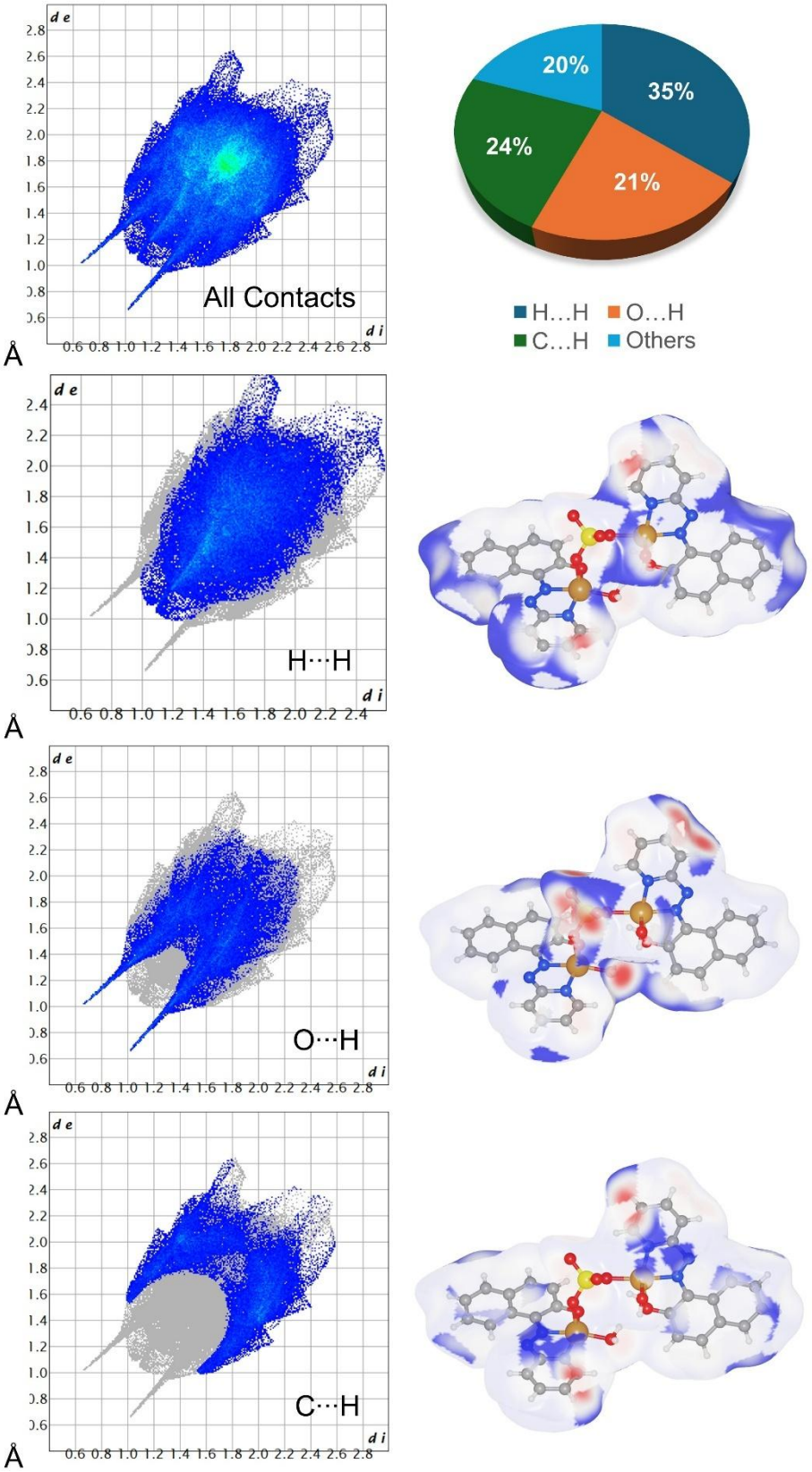

Figure S7. 2D fingerprint plots of all intermolecular contacts and the most prominent ones: H···H, O···H/H···O and C···H/H···C (left row). Corresponding Hirshfeld surfaces highlighting the d_{norm} patches associated with these specific interactions (right row). The chart illustrates the relative contributions (%) of different intermolecular interactions to the overall Hirshfeld surface.

5. Magnetic characterization

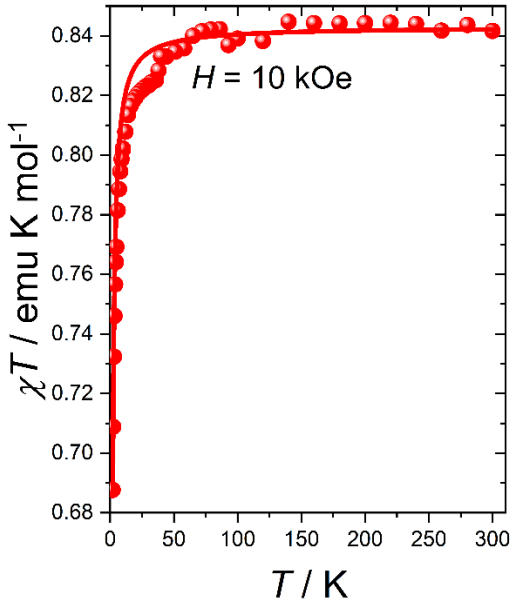

Figure S8. χT vs T recorded at H = 10 kOe. Dots are experimental data while solid line represents the best fit simulation as described in main.

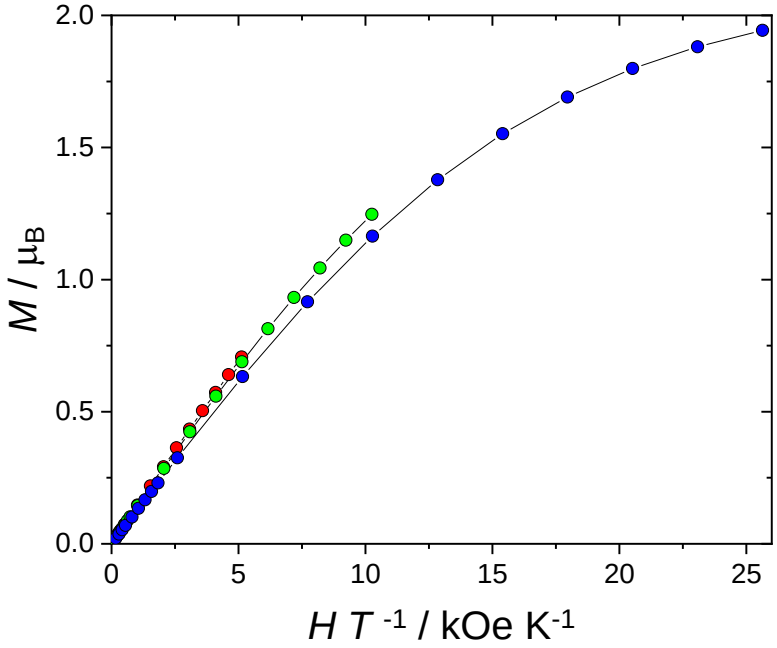

Figure S9. Reduced magnetization plots. The curves are almost superimposable, confirming a relatively low anisotropy. Dots are experimental data while solid lines are guide to the eye.

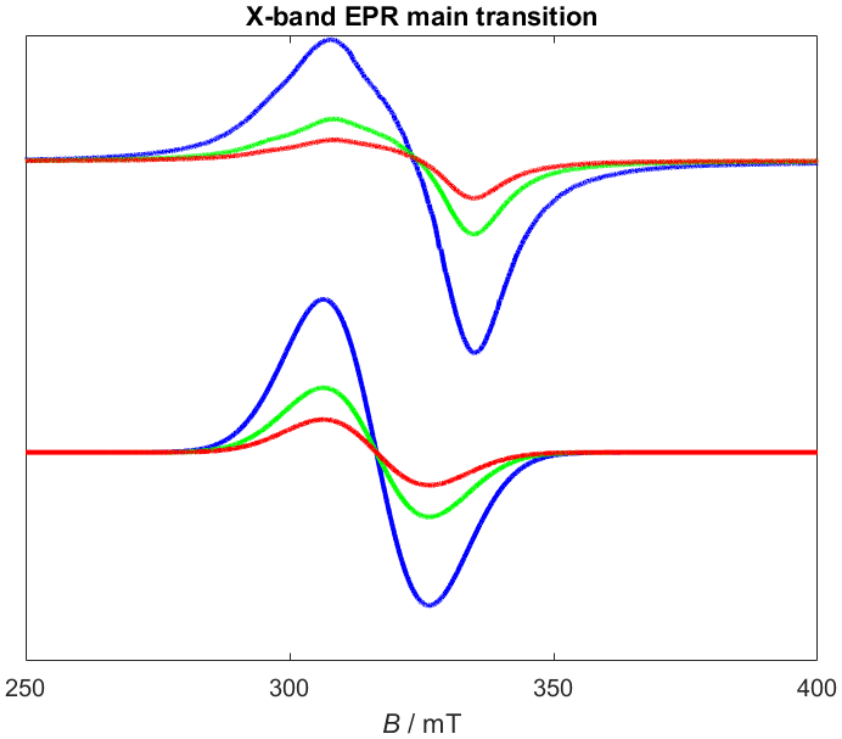

Figure S10. X-band EPR spectrum of $[Cu_2(\mu\text{-}SO_4)(PAN)_2(H_2O)_2]$. The top line is the experimental and the bottom line is the simulation using the parameters reported in the main text. The blue, green and red colours refer to T = 4, 10 and 20 K, respectively.

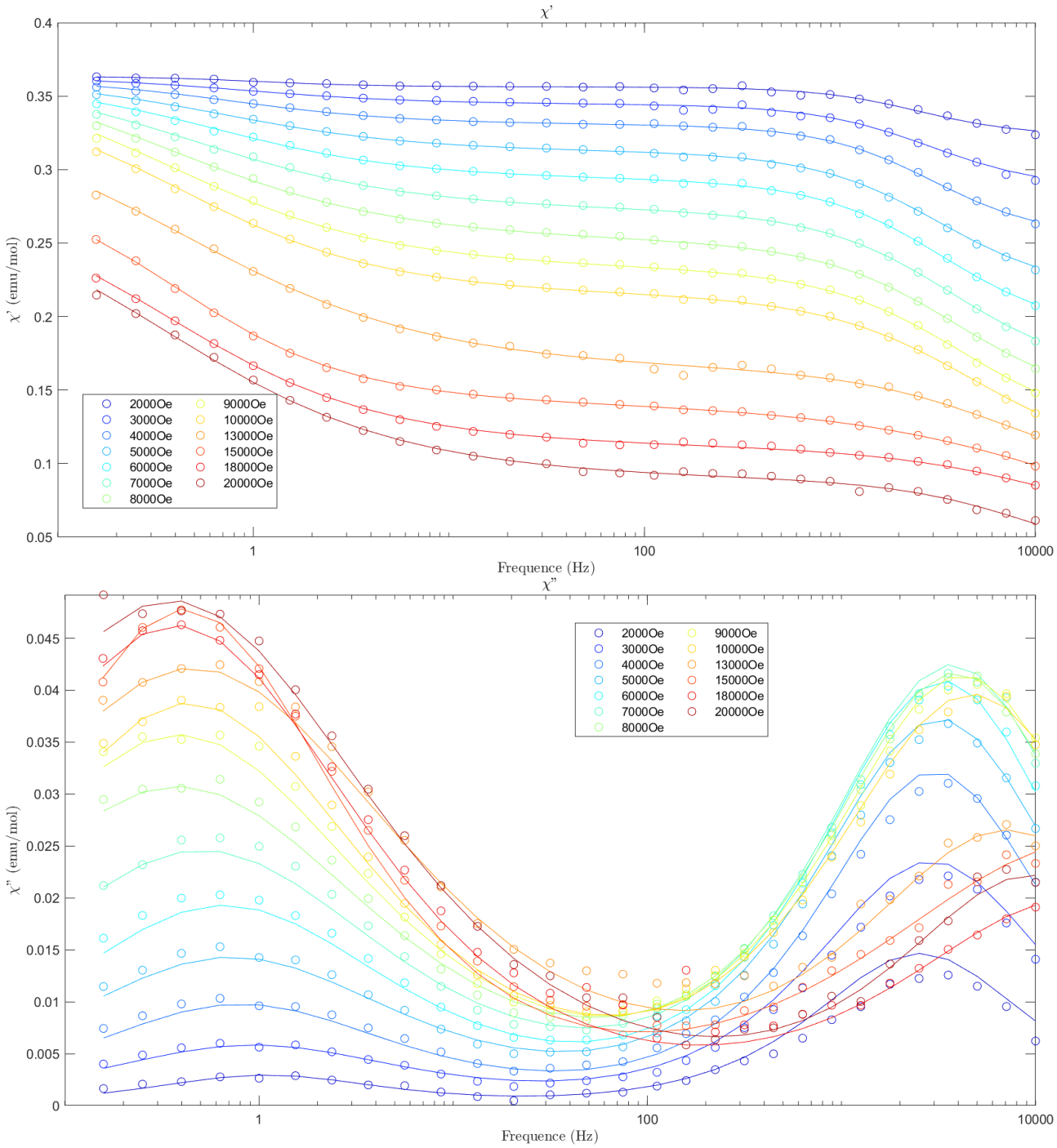

Figure S11. χ' and χ'' components of the ac susceptibility recorded at T = 2 K and various fields. The dots are the experimental points and the lines represent the best fit.

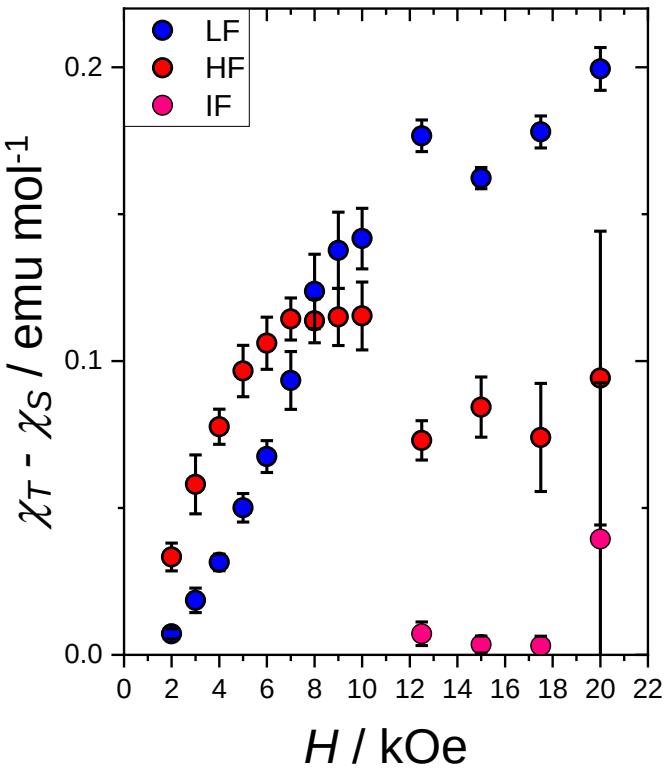

Figure S12. χT – χS values of the active processes at T = 2 K and various fields.

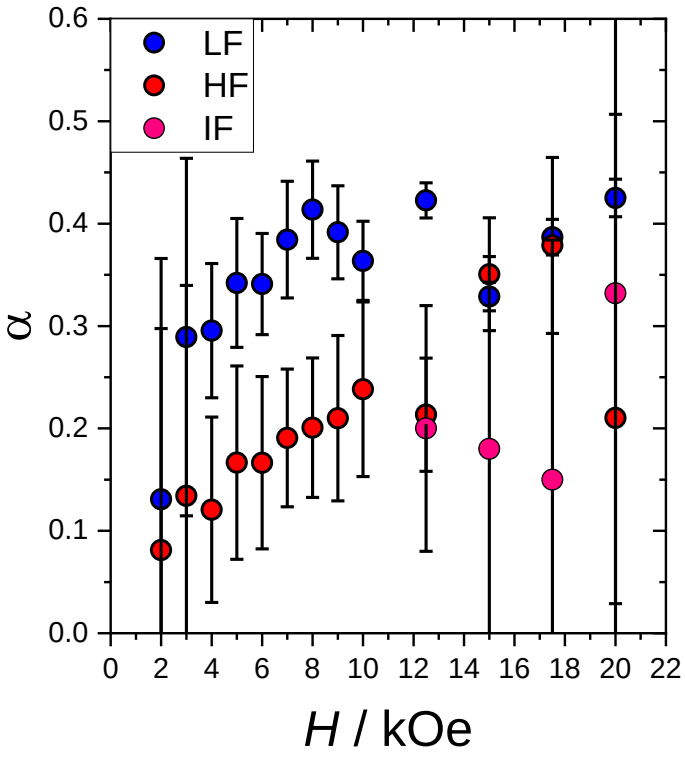

Figure S13. α values of the active processes at T = 2 K and various fields.

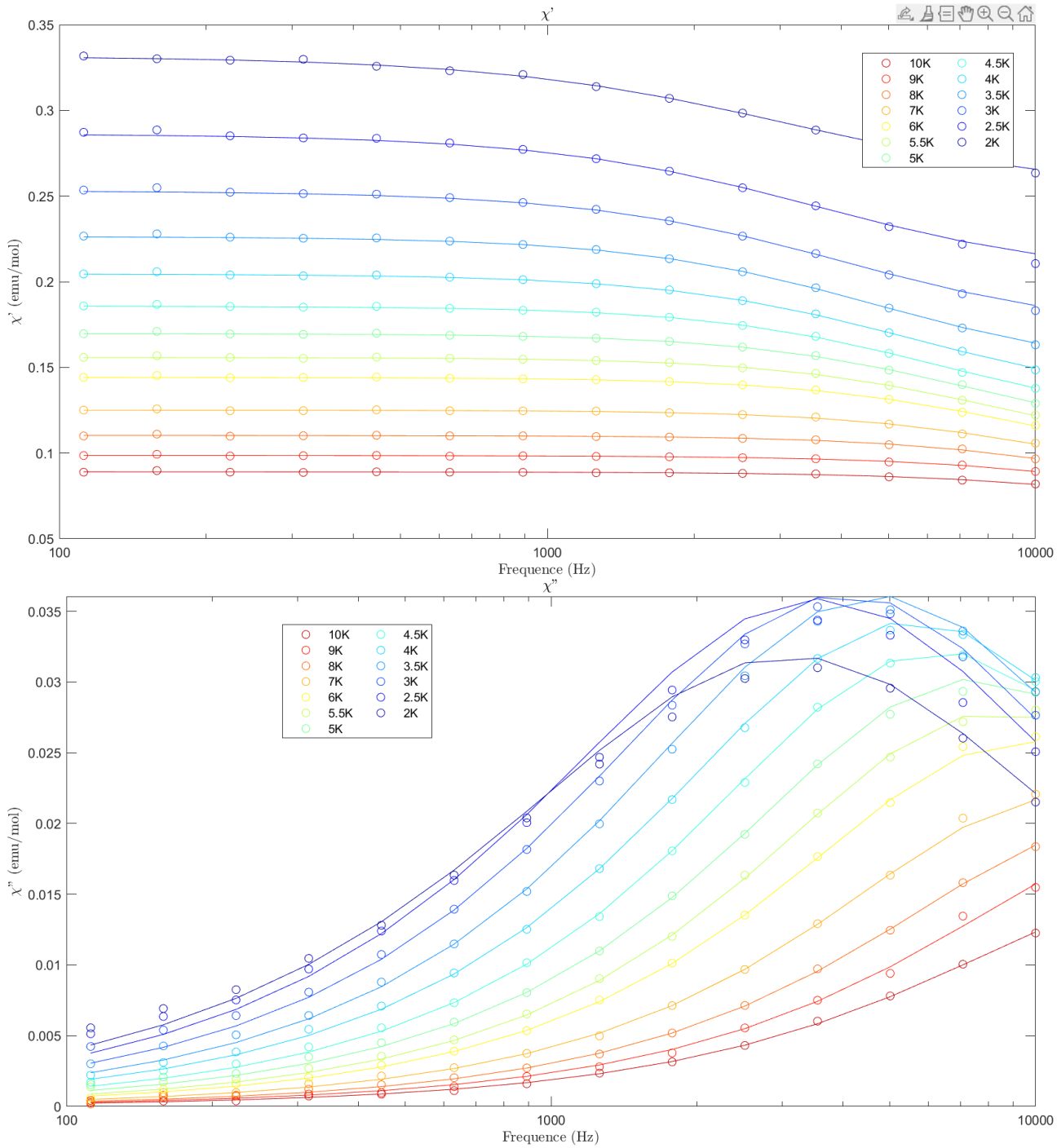

Figure S14. χ' and χ'' components of the ac susceptibility recorded at H = 4 kOe and various temperatures. The dots are the experimental points, and the lines represent the best fit.

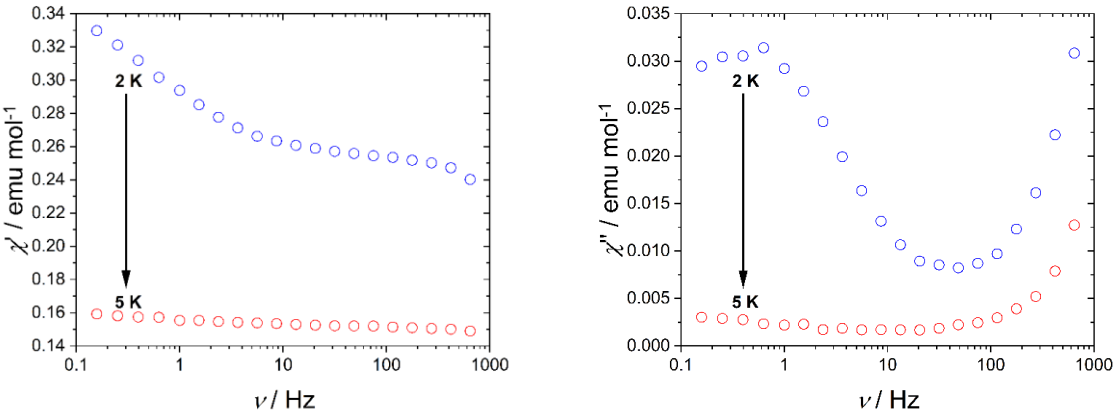

Figure S15. χ' and χ'' components of the ac susceptibility recorded at H = 8 kOe and T = 2, 5 K focused on the LF region.

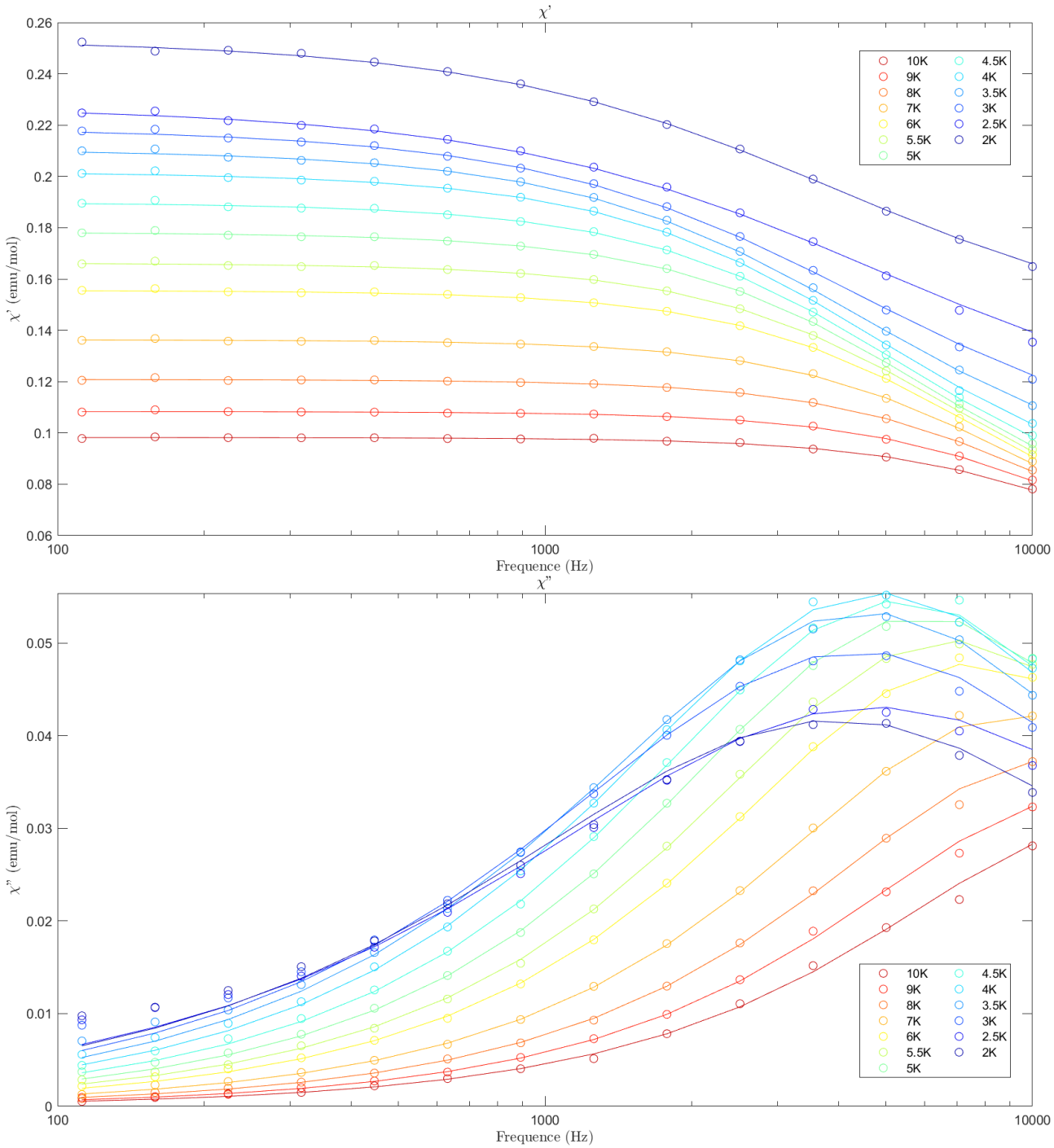

Figure S16. χ' and χ'' components of the ac susceptibility recorded at H = 8 kOe and various temperatures. The dots are the experimental points and the lines represent the best fit.

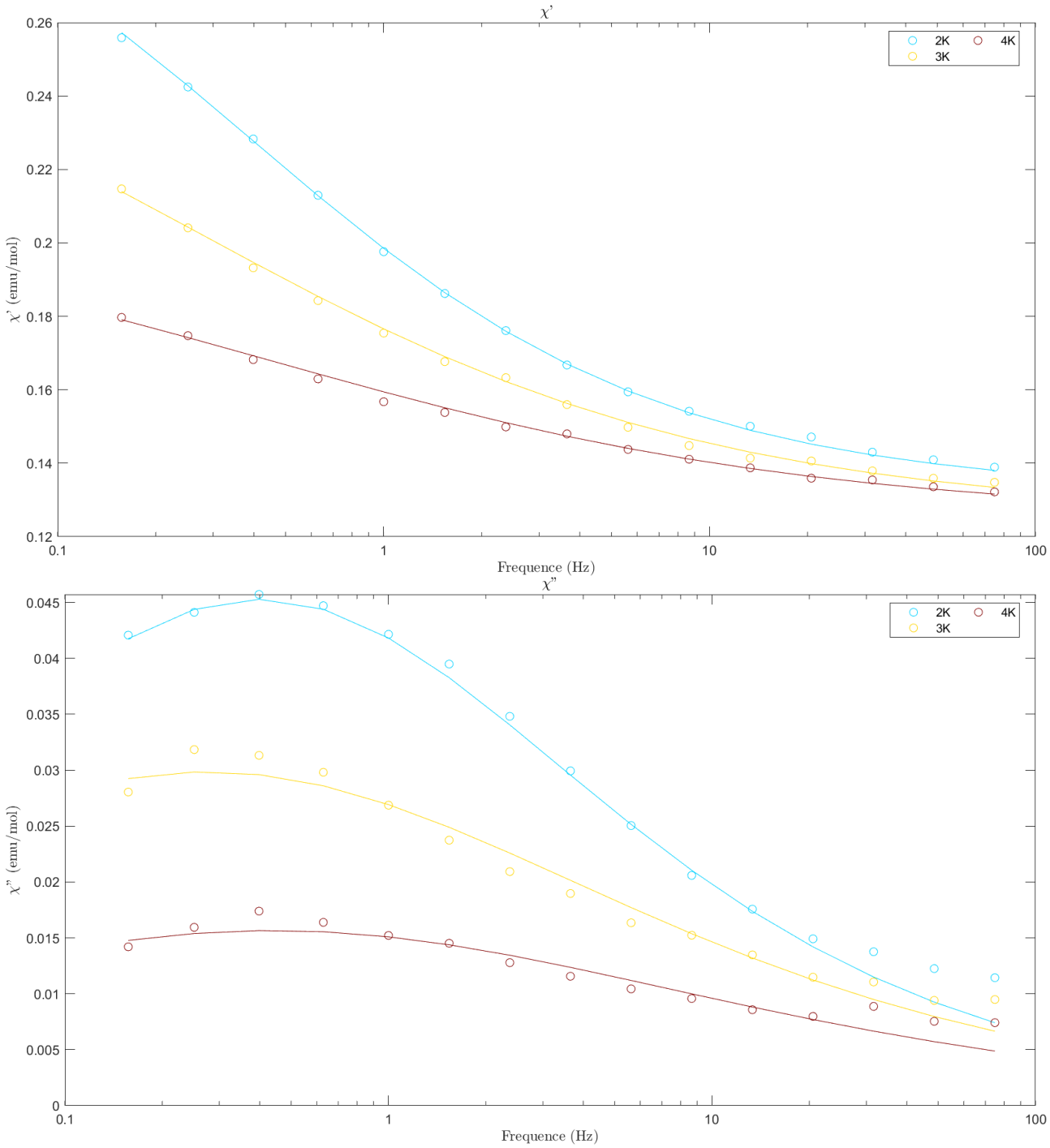

Figure S17. χ' and χ'' components of the ac susceptibility recorded at H = 15 kOe and various temperatures. The dots are the experimental points and the lines represent the best fit.

References

(1) S. Basu, S. Halder, I. Pal, S. Samanta, P. Karmakar, M.G. Drew, S. Bhattacharya. *Polyhedron*, 2008, ***27***(13), 2943-2951.

(2) B. Machura, J. Mroziński, R. Kruszynski, J. Kusz. *Polyhedron*, 2008, ***27***(13), 3013-3019.

(3) M. Pallab, A. Hens, S. Basak, K.K. Rajak. *Dalton Trans.*, 2013, ***42***(5), 1536-1549.

(4) W.B. Yu, Q.Y. He, H.T. Shi, Y. Pan, X. Wei. *Dalton Trans.*, 2014, ***43***(32), 12221-12227.

(5) K. Pramanik, B. Adhikari. *Polyhedron*, 2010, ***29***(3), 1015-1022.

(6) S.I. Ooi, D. Carter, Q. Fernando. *Chem. Commun.*, 1967, ***24***, 1301-1302.

(7) H. Adams, R.M. Bucknall, D.E. Fenton, M. Garcia, J. Oakes, J. *Polyhedron*, 1998, **17**(23-24), 4169-4177.

(8) W.B. Yu, Q.Y. He, X.F. Ma, H.T. Shi, X. Wei. *Dalton Trans.*, 2015, ***44***, 351.

(9) H. Wada, M. Shiro, A. Yuchi, G. Nakagawa. *Bull. Chem. Soc. Jpn*, 1988, ***61***(11), 3869-3875.

(10) T.F. Liu, H.Y. Lv, B.T. Zhao, J.G. Wang. *Structure Reports*, 2007, **63**(9), 2406.

(11) G.R. Desiraju, H. R. Luss, D.L. Smith. *J. Am. Chem. Soc.*, 1978, ***100***(20), 6375-6382.

(12) M. Shao, X. Dong, Y. Tang. *Sci. China, Ser. B*, 1988, ***31***, 789.

(13) Y. Wu, J. Wang, X. Kong, C. Sheng, R. Wang, N. Peyghambarian, Z. Zheng. *Inorg. Chim. Acta*, 2011, ***370***(1), 346-352.

(14) C. Wang, N. Jiao, L. Jun, M. Xiaoxun. *Inorg. Chim. Acta.*, 2017, ***464***, 81-87.

(15) G.M. Sheldrick. *Acta Crystallogr. A, Found. Crystallogr.*, 2015, ***71***(1), 3-8.

(16) G.M. Sheldrick. *Acta Crystallogr., Sect. C: Cryst. Struct. Commun.*, 2015, ***71***(1), 3-8.

(17) O.V. Dolomanov, L.J. Bourhis, R.J. Gildea, J.A. Howard and H. Puschmann, *J Appl Crystallogr.*, 2009, ***42***, 339-341.

(18) C.F. Macrae, L.I. Sovago, S.J. Cottrell, P.T. Galek, P. McCabe, E. Pidcock, M. Platings, G.P. Shields, J.S. Stevens, M. Towler. *J. Appl. Crystallogr.*, 2020, ***53***(1), 226-235.

(19) P. R. Spackman, M. J. Turner, J. J. McKinnon, S. K. Wolff, D. J. Grimwood, D. Jayatilaka, M. A. Spackman, *Applied Crystallogr.*, 2021, ***54***, 1006–1011.

(20) R. Herchel, I. Nemec, M. Machata, Z. Travnicek, *Inorg. Chem.*, 2015, ***54***, 8625–8638.

(21) H. Li, S.-G. Zhang, L.-M. Xie, L. Yu and J.-M. Shi, *J. Coord. Chem.*, 2011, ***64***, 3595–3608.